mAbs

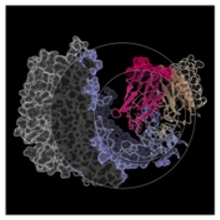

ISSN: 1942-0862 (Print) 1942-0870 (Online) Journal homepage: www.tandfonline.com/journals/kmab20

Structure-guided design of antibody CDRs to reduce their reactivity to treatment-emergent anti-drug antibodies

Maria U. Johansson, Anne Kerschenmeyer, Alessandra Carella, Simon Carnal, Yannik Schmidt, Alessandra de Felice, Dana Mahler, Marc Thomas, Fabio Mario Spiga, Julia Tietz, Christopher Weinert, Christian Hess, David Urech & Stefan Warmuth

To cite this article: Maria U. Johansson, Anne Kerschenmeyer, Alessandra Carella, Simon Carnal, Yannik Schmidt, Alessandra de Felice, Dana Mahler, Marc Thomas, Fabio Mario Spiga, Julia Tietz, Christopher Weinert, Christian Hess, David Urech & Stefan Warmuth (2026) Structure-guided design of antibody CDRs to reduce their reactivity to treatment-emergent anti-drug antibodies, mAbs, 18:1, 2604353, DOI: 10.1080/19420862.2025.2604353

To link to this article: https://doi.org/10.1080/19420862.2025.2604353

MABS
2026, VOL. 18, NO. 1, 2604353
https://doi.org/10.1080/19420862.2025.2604353

Taylor & Francis
Taylor & Francis Group

REPORT

Structure-guided design of antibody CDRs to reduce their reactivity to treatment-emergent anti-drug antibodies

Maria U. Johansson[a], Anne Kerschenmeyer[a], Alessandra Carella[a], Simon Carnal[a], Yannik Schmidt[a], Alessandra de Felice[a], Dana Mahler[b], Marc Thomas[c], Fabio Mario Spiga[a], Julia Tietz[d], Christopher Weinert[a], Christian Hess[a], David Urech[a], and Stefan Warmuth[a]

[a]Numab Therapeutics AG, Horgen, Switzerland; [b]Luzern, Switzerland; [c]OFLC, PSI, Villigen, Switzerland; [d]Institute of Physiology, University of Zürich, Zürich, Switzerland

ABSTRACT

Immunogenicity prediction is widely used in the developability assessment of antibodies, and many marketed and clinical-stage therapeutics have a predicted T-cell epitope in the second complementary-determining region of their light chain (CDR2L). To investigate such CDR2Ls in more detail, we identified an antibody with a CDR2L for which a patient had developed treatment-emergent (TE) anti-drug antibodies (ADAs) in a clinical setting. With this, we establish the importance of predicted T-cell epitopes in CDR2L. In the course of deleting the T-cell epitope, we decided to aim for a solution that can be applied broadly to facilitate larger high-throughput discovery campaigns. For this purpose, we have developed a double-mutation scheme that targets AHo67 (Kabat51) and AHo68 (Kabat52) in the CDR2L. This 67G-68G mutation scheme was applied to all light chain sequences of a tri-specific single-chain diabody fused to a single-chain variable fragment (scMATCH3™) antibody for which TE ADAs had been observed. Analyses of patient sera showed that introduction of 67 G-68 G in CDR2L in combination with our previously described T101S-T146K (Kabat: T87S-T110K) framework mutations led to a scMATCH3 antibody with significantly reduced levels of both preexisting and TE ADA reactivities. For a diverse collection of single-chain variable fragments, application of the 67 G-68 G mutation scheme was experimentally seen to not substantially affect the functional or biophysical properties of the molecules, suggesting that this mutation scheme may be applicable to the improvement of therapeutic safety of antibodies of many types, with CDR2L-associated immunogenicity.

ARTICLE HISTORY
Received 24 August 2025
Revised 16 November 2025
Accepted 6 December 2025

KEYWORDS
Anti-drug antibodies; antibody; antibody fragment; biotherapeutics; immunogenicity; multispecific; scFv

Introduction

Immunogenicity is defined as follows by the United States Food and Drug Administration (FDA)[1]:«*Immunogenicity is the propensity of a therapeutic protein product to generate an immune response to itself, a related structure, or product complex; and/or to induce immunologically related adverse clinical events.*»

The presence of anti-drug antibodies (ADAs)[2] poses a significant challenge in the design and development of biologic therapies. Biologics, including therapeutic antibodies and antibody fragments, may provoke immune responses (*i.e.*, exhibit immunogenicity) by triggering the immune system to generate ADAs that can be either neutralizing or non-neutralizing.[3] It is common to distinguish between treatment-emergent (TE) ADAs, which arise in response to treatment, and preexisting (PE) ADAs, which are present in a patient prior to treatment.[3] The onset time of TE ADAs can vary considerably between patients, with detection reported as early as four weeks[4,5] and up to three to six months[6] following treatment initiation. The consequences of anti-drug immunogenic reactions span from no effect to life-threatening responses,[7–9] and detailed guidelines exist on how to perform immunogenicity assessments during drug development.[10,11]

While there are treatment[12–20] and patient-associated[15–17,21–23] factors that can influence ADA formation, given the far-reaching consequences of immunogenicity, it is desirable to reduce these risks as much as

CONTACT Stefan Warmuth s.warmuth@numab.com; Maria Johansson m.johansson@numab.com Numab Therapeutics AG, Bachtobelstrasse 5, Horgen CH-8810, Switzerland

Supplemental data for this article can be accessed online at https://doi.org/10.1080/19420862.2025.2604353.

possible in the early discovery and preclinical development process. Reducing immunogenicity risks of biologics typically involves identifying and eliminating amino acid sequence-related causes that can influence molecular factors and properties such as aggregation propensity,[24,25] isoelectric point (pI) imbalances,[26] susceptibility to posttranslational modifications (PTMs),[27,28] and the presence of B- and T-cell epitopes.[29,30]

B-cell epitopes, which comprised solvent-exposed amino acids on the intact surface of biologics, are difficult to accurately identify using computational methods. Conversely, the presence of T-cell epitopes, which are believed to correlate with peptide fragments of the biologics being high-affinity binders of major histocompatibility complex (MHC) class II,[31–34] can be detected using computational means. Although not accounting for all complex processes involved, computational predictors of MHC class II binding have proven to be sufficiently accurate,[33,35] and are widely used despite it being well known that many MHC class II binding peptides predicted are false positives.[36] False positives are due to methods not properly accounting for antigen processing, T-cell receptor recognition of the MHC class II/peptide complex, or T-cell activation.[2,37] In contrast, the MHC class I binder prediction problem has proven easier, and current methods are able to predict MHC class I binding with very high accuracy.[38]

Experimental procedures to identify immunogenic sequences in biologics can be labor and resource intensive and often yield ambiguous results. In a previous study, we analyzed instances of PE ADA reactivity, and identified mutations that reduce or eliminate PE ADA reactivity for single-chain variable fragments (scFv).[39] In the current study, we used an observed clinical instance of TE ADAs to establish the clinical relevance of predicted T-cell epitopes in the second complementary-determining region of the light chain (CDR2L), and developed effective deimmunization procedures for removal or substantial reduction of predicted T-cell epitope content. In addition to the removal of the clinically observed immunogenicity, we have developed a different solution for the removal of similarly located T-cell epitopes that appears to be applicable to a wide range of antibodies. Thereby, we provide a means to obtain Fv fragments with good biophysical properties and reduced immunogenicity for assembly into bispecifics and multispecifics.

After having identified the immunogenic sequence as being located in the complementary-determining regions (CDRs), more specifically CDR2L, in the tri-specific antibody employed in the mentioned clinical setting, we applied computational mutagenesis and MHC class II binding predictions to find mutation schemes that will not trigger TE ADA formation. Similar to Cassotta *et al.*, who identified and removed a T-cell epitope in the CDR2L region of Natalizumab,[40] we searched for and found mutations uniquely tailored to the CDR2L amino acid sequence that had been identified as being the likely cause of the TE ADAs, and that eliminate their binding. Having achieved this first objective and intent on improving the procedure of Cassotta *et al.*, we were, additionally, able to successfully identify a mutation scheme to remove predicted T-cell epitope content, irrespective of the CDR2L amino acid sequence.

Results

ADA assays

A direct assay to detect ADAs in human serum has been described previously,[39] whereby two measurements (screening and confirmatory) are performed for each test molecule. For such assays, a decrease of the absorbance signal in the spiked well indicates that the signal observed in the unspiked well of the initial screening assay is specific to the molecule coated on the plate (see Materials and Methods). Such decreases of the absorbance signal are reported as relative inhibition (in the confirmatory assay) of the absorbance obtained in the screening assay. Thus, the lower the absorbance in the spiked well is, compared to the unspiked well, the higher the relative inhibition is. Additionally, it is important to note that while we have previously[39] described a strategy to eliminate PE ADAs binding to the scFv framework (by application of T101S-T146K), the parental tri-specific single-chain diabody fused to a single-chain variable fragment (herein referred to as scMATCH3™, rather than scDb-scFv) under investigation did not include the described mutations.

The absorption signals obtained at different treatment days for scMATCH3 tested against one patient's serum samples are shown in Figure 1(A). Higher absorption levels indicate a higher serum-derived antibody binding to the scMATCH3. Figure 1(A) reveals TE ADAs against scMATCH3 present in patient serum

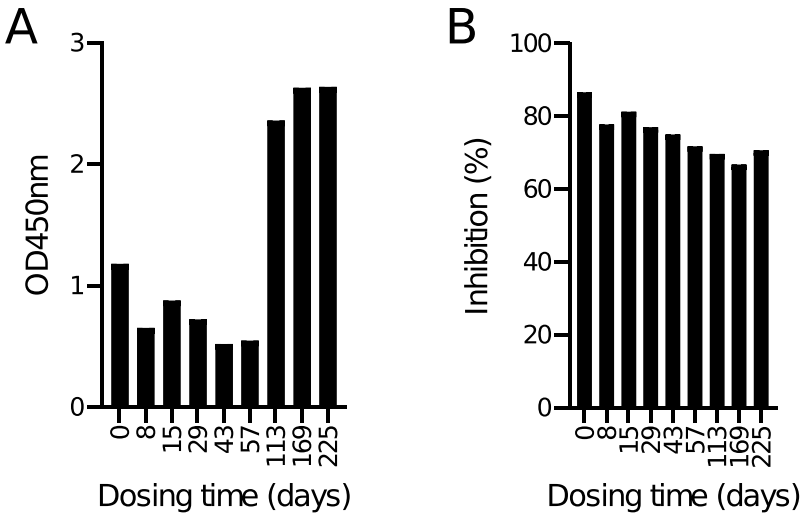

Figure 1. (A) Absorption signals for PE ADA and TE ADA reactivities against scMATCH3 for samples from one patient from day 1 to day 225, determined with the ELISA-based ADA binding assay. Absorption levels were measured at 450 nm and are given in A.U. (B) ELISA-based ADA binding assay depicting inhibition of absorption signals from day 1 to day 225 after spiking the serum from one patient with scMATCH3 (150 nM spiking).

samples collected *after* 57 days treatment. The absorbance signals seen for samples collected *up to* 57 days indicate the presence of some PE ADAs against scMATCH3. In Figure 1(B), the ADAs shown to be detected in Figure 1(A) (both PE and TE ADAs) are indeed specific to scMATCH3, since inhibition values are high. The PE ADAs observed in Figures 1(A,B) would not have been present with the mutations (T101S-T146K) to prevent PE ADA reactivities.[39] Later, the effect of said mutations to remove PE ADAs will be seen in Figure 6(C). Hereafter, in all figures showing ADA binding assay data, we only present the confirmatory part of assays.

Localization of the te ADA epitope

Figure 2 summarizes the experiments performed to identify which of the scFv building blocks provoked the formation of TE ADAs. Again, in this case, the mutations described previously to eliminate PE ADAs were not included in scMATCH3. This explains the ability of the control scFv, which also lacks T101S-T146K, to inhibit ADA binding to the scMATCH3 for samples derived up to 57 days after treatment starts. For patient-derived sera from later time points, the control scFv, does not inhibit ADA binding, and since the control scFv has the same framework as scFvs 1–3, this indicates formation of scMATCH3 CDR specific TE ADA. For scFv3, but not for scFv1 or scFv2, an inhibition of scMATCH3 specific TE ADAs is observed, identifying one or more of the scFv3 CDRs as the TE-ADA epitope within the scMATCH3.

Subjecting the amino acid sequence of scFv3 to MHC class II binding prediction yields a median percentile rank (of 27 alleles) for each contiguous 15mer sub-sequence (Figures 3(A,B)) and is sometimes referred to as a T-cell epitope prediction profile. The reference set of 27 alleles used in this study are considered to cover more than 98% of individuals in all major ethnicities worldwide.[41]

As can be seen in Figure 3(A), the CDR2L region (15mer indices in the approximate range 40 – 50) of scFv3 exhibits a very deep and broad cluster of 15mers with low median percentile ranks, which is indicative of a distinct likelihood of MHC class II binding.[42] However, no other region of scFv3, including the variable heavy chain (VH), shown in Figure 3(B), exhibits similarly distinct likelihood of MHC class II binding. Figure 3(C) shows the percentile rank for each of the 27 MHC class II alleles as a heatmap for 15mer indices in the range 36 – 56. For each 15mer sub-sequence MHC class II allele pair, the binding core 9-mer is indicated by a symbol when it is one that contributes to the cluster of 15mers with low median percentile ranks (indices 42 – 51).

It is relevant to note that, henceforth, molecule designs are distinguished by the amino acid sequence of the CDR2L region, written in upper case (*e.g.*, RASILAS, RAKDLAS, *etc.*).

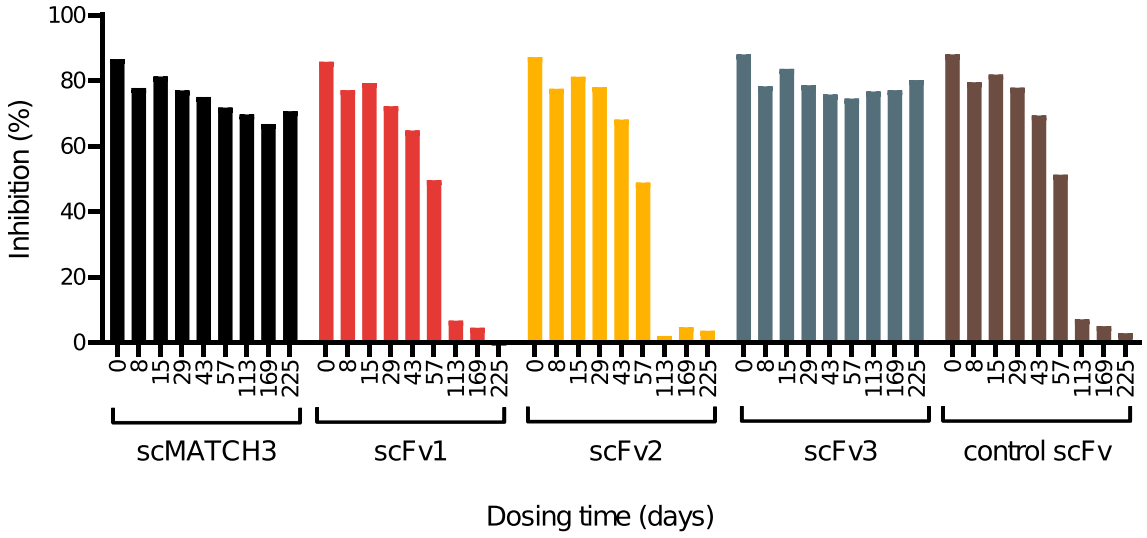

Figure 2. Results of ADA binding assays (inhibition of absorption signals) from day 1 to day 225 after spiking the serum from one patient with scMATCH3 (first panel), as well as the individual scFv components of scMATCH3, namely, scFv1 (second panel), scFv2 (third panel) and scFv3 (fourth panel), as well as a control scFv (fifth panel). The control scFv has a CDR set different from the CDR sets of scFv1, scFv2, and scFv3, on the same framework (i.e., human Vk1-VH3 type) and was not used for treatment of the patients. Spiking concentrations were 150 nM for scMATCH3 and 450 nM spiking for all scFvs.

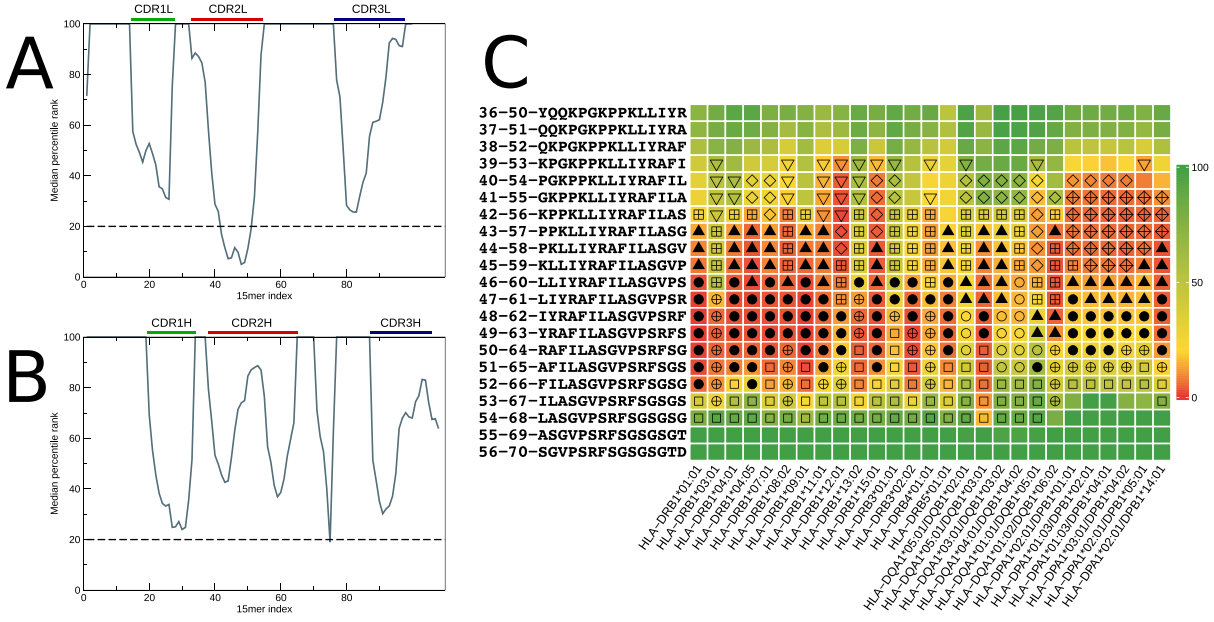

Figure 3. T-cell epitope prediction profiles (defined in material and methods [T-cell epitope content predictions]) for the (A) VL domain of scFv3 and the (B) VH domain of scFv3. The median percentile rank of 20, is indicated by a dashed line. (C) Heatmap of the percentile rank for each of the 27 MHC class ii alleles for 15mer indices in the range 36 – 56. For each [15mer index:MHC class ii allele]-pair, the binding core 9-mer is indicated by a symbol when it is one that contributes to the cluster of 15mers with low median percentile ranks (15mer indices 42 – 51). In decreasing order, the contributions to the cluster are as follows: FILASGVPS (32.3%, ●), YRAFILASG (25.9%, ▲), IYRAFILAS (11.0%, ⊞), LIYRAFILA (10.0%,), ILASGVPSR (8.5%, ⊕), LASGVPSRF (5.0%, □) LLIYRAFIL (4.5%, ◇), AFILASGVP (2.0%, ○) and KLLIYRAFI (1.0%, ▽).

Judging from our examination of known clinical-stage therapeutics (CSTs) sequences (*vide infra*), the introduction of a human germline sequence in CDR2L may well have been used as a deimmunization strategy for some of these CSTs. Consequently, a first attempt at removing the TE ADA epitope was to substitute the CDR2L sequence (RAFILAS) of scFv3 with a human V*k*1 germline sequence, AASSLQS (human Vk1_39, same as Vk1 consensus), which does indeed eliminate TE ADA binding (Figure 4(A), second panel), and

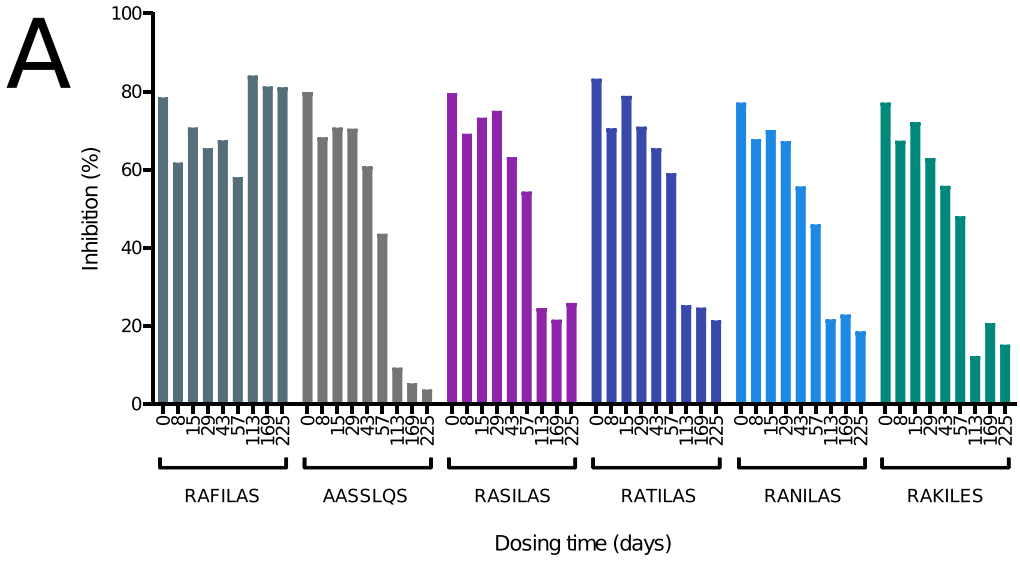

B

CDR2L sequence	mutation count	AHo58 residue	net charge	cluster count	cluster size	15mer hotspot sequence	15mer hotspot median percentile rank	T_m (°C)	K_D (M)	K_D ratio to RAFILAS
RAFILAS	0	R	1	1	10	48-62-IYRAFILASGVPSRF	5.01	73.0	1.13E-11	1.0
RASILAS	1	R	1	1	8	44-58-PKLLIYRASILASGV	5.17	75.0	2.72E-11	2.4
RATILAS	1	R	1	1	8	44-58-PKLLIYRATILASGV	6.50	74.8	3.23E-11	2.9
RANILAS	1	R	1	1	8	44-58-PKLLIYRANILASGV	8.23	74.6	3.95E-11	3.5
RAKDLAS	2	R	1	0	0	NONE	NONE	72.8	1.30E-09	114.8
RAKILES	2	R	1	1	4	44-58-PKLLIYRAKILESGV	13.01	72.2	9.65E-11	8.5
RANNLAS	2	R	1	1	5	46-60-LLIYRANNLASGVPS	11.33	73.6	1.88E-10	16.6
RASTLAS (CST)	2	R	1	1	7	45-59-KLLIYRASTLASGVP	4.58	74.2	2.26E-10	19.9
RANDRAS	3	R	1	0	0	NONE	NONE	71.3	3.69E-10	32.5
RTKDLAS	3	R	1	0	0	NONE	NONE	72.0	8.62E-10	76.0
RAKDLQS	3	R	1	0	0	NONE	NONE	71.0	1.84E-09	162.6
RTSNLAS (CST)	3	R	1	1	5	44-58-PKLLIYRTSNLASGV	11.20	72.3	1.69E-10	14.9
RTNDRAS	4	R	1	0	0	NONE	NONE	69.7	5.91E-10	52.1
RANDRQS	4	R	1	0	0	NONE	NONE	69.8	5.50E-10	48.5
RANNRES	4	R	1	0	0	NONE	NONE	71.3	2.07E-10	18.2
RASDRQS	4	R	1	0	0	NONE	NONE	70.4	7.37E-10	64.9
RANRLVD (CST)	4	R	1	1	7	41-55-GKPPKLLIYRANRLV	5.29	74.2	3.56E-10	31.4
AASSLQS	4	A	0	0	0	NONE	NONE	68.2	NB	NA
RAFILAS	0	R	1	1	10	48-62-IYRAFILASGVPSRF	5.01	73.0	1.91E-11	1.0
RGGILAS	2	R	1	0	0	NONE	NONE	71.5	3.40E-11	1.8

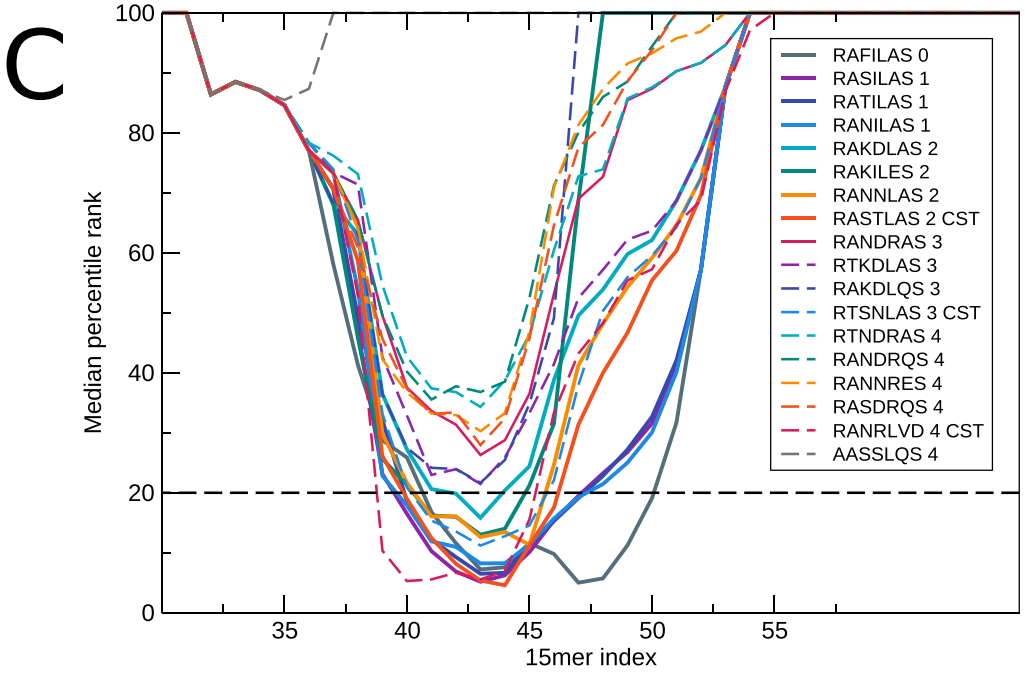

Figure 4. (A) The presence of CST inhibition of absorption signals from day 1 to day 225 after spiking the serum from one patient with scFv3 (450 nM) having different CDR2L sequences. From left to right the sequences are as follows: RAFILAS, AASSLQS, RASILAS, RATILAS, RANILAS and RAKILES. (B) CDR2L sequences with differences from RAFILAS indicated by red-colored symbols, depicted in tabular form. For sequences originating from a CST, this is indicated after the sequence. Values

thereby confirms that TE ADA are indeed directed specifically against the CDR2L region of scFv3 (*i.e.*, variable fragment (Fv) 3 in scMATCH3). However, with respect to thermal stability (T_m) and affinity (K_D), the substitution with AASSLQS leads to a reduction (−4.8°C) of the former and, as expected, to a complete loss of the latter (Figure 4(B)) further illustrating the importance of AHo58. The need to find a deimmunization solution that maintains the functional and biophysical properties led to an extensive investigation of CDR2L sequence variants.

Design and evaluation of alternative scFv3 CDR2Ls

After having identified the location of the epitope of the TE ADAs within scFv3's CDR2L, we performed MHC class II binding predictions for CDR2L replacement candidate sequences to identify mutations that reduce the predicted T-cell epitope content. To obtain the CDR2L replacement candidate sequences, we were inspired by human and rabbit germline sequences, CST sequences, and in-house rabbit sequences. Additionally, CDR2L replacement candidate sequences were generated combinatorially. The first CDR2L position in Honegger (AHo) numbering is AHo58 (Kabat50), and for combinatorially generated CDR2L replacement sequences, AHo58 was retained from RAFILAS as an arginine – since AHo58 is often involved in CDR1L, CDR3H, and antigen contacts, and has a high somatic mutation rate. The details elaborating these findings are outlined in the following section, "Design and evaluation of a broadly applicable CDR2L mutation scheme," and Figure 5. For the remaining six positions (AHo67-AHo72), amino acid sequences were generated using residue types with high frequencies of occurrence at each corresponding position in in-house rabbit antibody sequences. In total, MHC class II binding predictions were performed for 1461 different CDR2L sequences, inserted into to the parental scFv3 that had exhibited TE ADA reactivity. Out of these CDR2L sequences, 16 sequences were selected, where AHo85 was an arginine, they had the same net charge and a sequence identity of at least 3 to RAFILAS, and possessed a low predicted immunogenicity. In addition, three CDR2L sequences originating from CST sequences were chosen.

For the described MHC class II binding predictions, we began by looking at single mutations in the CDR2L region and could see that no single amino acid substitution was able to completely eliminate the predicted T-cell epitope content (Figure 4(C)). This is expected since the mentioned cluster of 15mers with low median percentile ranks is very deep and broad. Of the 1461 CDR2L sequences, the 16 plus 3 designs mentioned above – that had been evaluated for T-cell epitope content and various mutation counts (Figure 4(B)) – were produced. Nano differential scanning fluorimetry (nDSF) and surface plasmon resonance (SPR) revealed minimal impact on thermal stability and affinity, respectively. Graphs of corresponding median percentile rank versus 15mer index are shown in Figure 4(C). The most promising CDR2L designs, with respect to thermal stability and affinity, were tested on patient serum for TE ADA reactivity (Figure 4(A)). All single-mutation designs (RASILAS (third panel), RATILAS (fourth panel), and RANILAS (fifth panel)) depict a similar level of TE ADA reactivity; which is substantially reduced compared to the parental CDR2L (RAFILAS, first panel). In agreement with T-cell epitope content predictions (Figure 4(C)), the reduction in TE ADA reactivity for all single-mutation designs is lower than that for both the double-mutation design (RAKILES, sixth panel) and for human germline (AASSLQS, second panel). Furthermore, the reduction in TE ADA reactivity for RAKILES is lower than for AASSLQS. The high inhibition seen for early time points in Figure 4(A) is explained by the fact that the T101S-T146K mutation scheme was not applied to these sequences.

Although a CDR2L design such as RAKILES does efficiently reduce the TE ADA reactivity on patient serum, deriving mutations uniquely tailored to each CDR2L sequence with predicted T-cell epitope content

indicating their mutation count, AHo58 residue type, net charge, predicted T-cell epitope content (namely, cluster count, cluster size, 15mer hotspot sequence and 15mer hotspot median percentile rank), thermal stability, affinity and KD ratio to RAFILAS. (C) T-cell epitope prediction profiles (defined in material and methods [T-cell epitope content predictions]) for scFv3 VL domains with different CDR2L sequences. The median percentile rank of 20, is indicated by a dashed line. The line style and color of the profile for each sequence is shown in the legend box. The mutation count is shown after each sequence, and CST is indicated, when applicable.

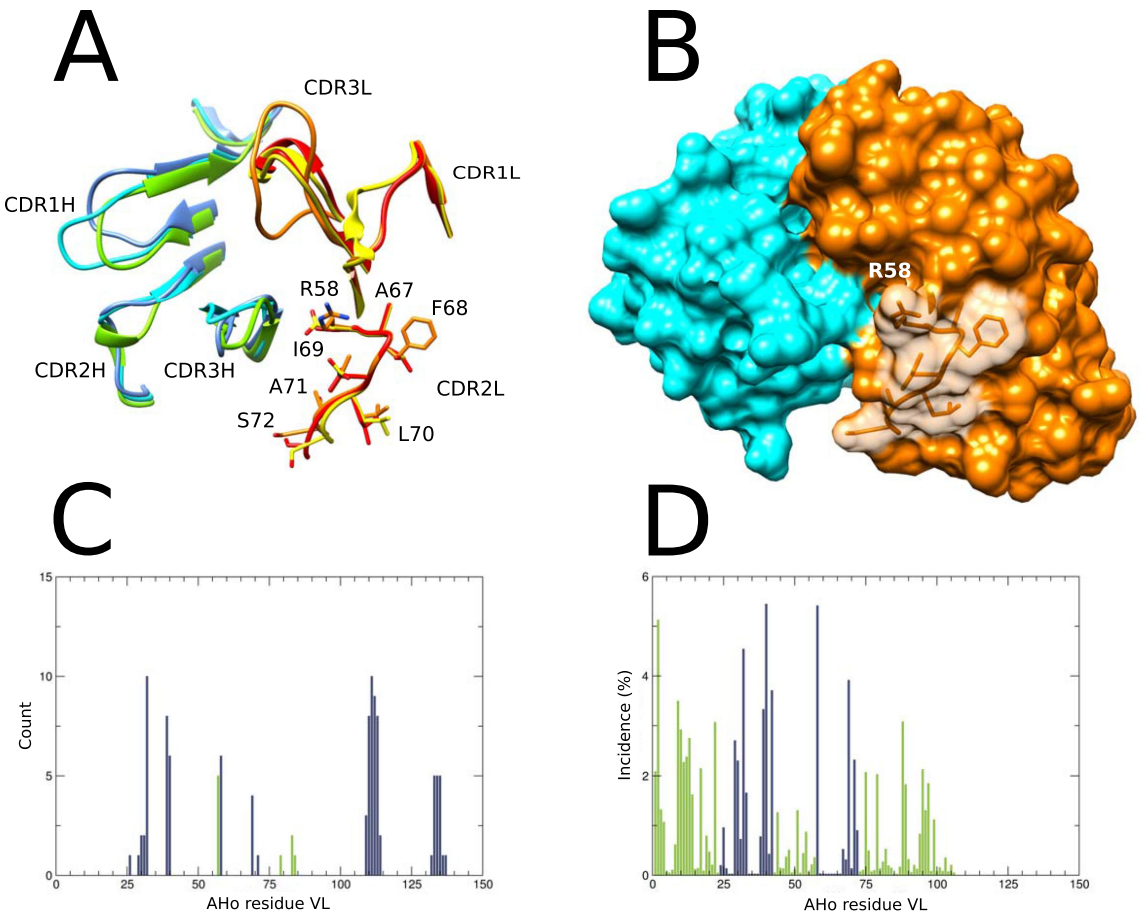

Figure 5. (A) Overlay of ribbon representations of scFv1 (yellow (VL) and green (VH)), scFv2 (red (VL) and blue (VH)), and scFv3 (orange (VL) and cyan (VH)) crystal structures. Labeling of sidechains of CDR2L residues uses AHo numbering. The corresponding Chothia/Kabat/IMGT numberings are: Arg50/50/56, Ala51/51/57 Phe52/52/65, Ile53/53/66, Leu54/54/67, Ala55/55/68, and Ser56/56/69. (B) Surface representation of the scFv3 (same coloring as in (a)) crystal structure with side chains of CDR2L residues shown in stick representation. (C) Antigen contact count for each AHo residue (VL) in a collection of 16 in-house and RCSB PDB rabbit antigen-antibody complex crystal structures. Bars for framework residues are indicated in green, whereas bars for CDR residues are indicated in blue. (D) Incidence of somatic mutations for each AHo residue (VL) for a collection of 1493 in-house rabbit antibody sequences. Bars for framework residues are indicated in green, while bars for CDR residues are indicated in blue.

is not an approach that can feasibly be applied at scale in antibody development. Therefore, we decided to search for a CDR2L mutation scheme that would both remove the very deep and broad RAFILAS cluster of 15mers in the CDR2L region of the scFv3, and be broadly applicable to CDR2L regions from human, mouse, rabbit, and preferably other species as well.

Design and evaluation of a broadly applicable CDR2L mutation scheme

Before making further attempts at deimmunizing the CDR2L region of scFv3 (and other CDR2L regions), we performed a detailed investigation of 16 in-house and Research Collaboratory for Structural Bioinformatics Protein Data Bank (RCSB PDB) rabbit antigen-antibody complex crystal structures (downloaded late 2020), as well as a collection of 1493 in-house rabbit antibody sequences. An overlay of the trispecific scMATCH3 components; scFv1, scFv2 and scFv3 is shown in Figure 5(A), where the similar conformations of CDR2Ls in scFvs with different target specificities can be clearly seen. Figure 5(B) presents a surface representation of scFv3, with the CDR2 highlighted in stick representation. The antigen-antibody contacts in the 16 in-house and RCSB PDB complexes are summarized in Figure 5(C), and the per-residue incidence of somatic mutations in the 1493 in-house rabbit antibody variable light chain (VL) sequences is shown in Figure 5(D). Collectively, this indicates that residue AHo58 (Kabat50) appears to be the most

important residue of CDR2L, by virtue of being involved in intra-chain contacts to CDR1L and inter-chain contacts to the functionally crucial CDR3H (Figures 5(A,B)). Moreover, AHo58 has frequent involvement in antigen contacts (Figure 5(C)) and is the position with the highest number of somatic mutations (Figure 5(D)). Consequently, as noted previously, we kept AHo58 unchanged in all our CDR2L designs and refrained from altering the net charge of the CDR2L in these designs.

As already mentioned, a single mutation is not enough to eliminate the cluster of 15mers in CDR2L with low median percentile ranks and, therefore, we wanted to find the least invasive double-mutation scheme. Similar to AHo58, AHo69 (Kabat53) is frequently involved in antigen contacts and often subject to somatic mutations and was, therefore, also not a suitable candidate for mutation (Figures 5(C,D)). Residues AHo67 (Kabat51) and AHo68 (Kabat52) are both highly conserved among rabbit and human Vk germline sequences and are contained in CDR2L in all common CDR definitions (Chothia: 3, IMGT: 3, Kabat: 7). Targeting these two residues may appear counter-intuitive. However, in the setting of antibody CDRs, we believe not infringing upon sequence adaptability is important, and a mutation scheme that targets conserved positions is much more likely to be widely applicable. For all these reasons we decided to investigate mutations of AHo67 and AHo68.

To find a mutation scheme for AHo67 and AHo68 with broad applicability, T-cell epitope content predictions were performed for all in-house CDR2L sequences inserted into human IGKV1-39 frameworks. As a filtering criterion we choose to fix AHo58 to one of the following residues: R, S, K, G, D, A, Q, Y, E, L and T, corresponding to the most frequently occurring AHo58 residue types in the 1493 inhouse rabbit sequences. Subsequently, we applied all possible residue substitutions on AHo67 and AHo68, excluding C, P, H, and larger hydrophobic residues such as I, L, M, F, Y and W, and such that a change in net charge of the CDR2L was avoided. Reduction of predicted T-cell epitope content across a large subset of all tested sequences was observed for a few distinct mutation schemes (*i.e.*, AHo67, AHo68 mutation target residue pairs).

For each mutation scheme where predicted T-cell epitope content was reduced across a large subset of all tested sequences, we identified rabbit antibody crystal structures (in-house and RCSB PDB) that had CDR2L sequences such that AHo58 was identical to AHo58 in a sequence for which T-cell epitope content was predicted. Additionally, the sequence identity for AHo69, AHo70, AHo71, and AHo72 between the same two sequences was as high as possible. The structural feasibility of each mutation scheme was then assessed by performing computational mutagenesis calculations using the Rosetta software[43] on all structures identified as described. From these structural feasibility assessments, 67 G-68 G emerged as the least destabilizing mutation scheme. Note, however, that when AHo58 is an aspartic acid, 67 G-68 G would introduce an isomerization (DG) PTM. In such cases, substitution by a human germline is likely better. When AHo58 is an asparagine (a rare case in the in-house rabbit antibody sequences), 67 G-68 G would introduce a deamidation (NG) PTM.

Nonetheless, 67 G-68 G (Figure 6(A)) was the most promising structurally feasible double-mutation scheme identified, and it also has the beneficial property of not introducing any new PTMs in the most frequent rabbit CDR2Ls. Furthermore, 67 G-68 G leads to DG or NG PTMs in only 16.3% of the 962 VL sequences of CSTs described in more detail below. Graphs of the median percentile rank versus 15mer index, before and after the application of 67 G-68 G, are shown in Figure 6(A).

To evaluate the 67 G-68 G double-mutation scheme for reduction of TE ADAs in combination with our previously described double-mutation scheme (T101S-T146K) for reduction of PE ADAs,[39] both pairs of double-mutations were first applied to scFv3 and seen to efficiently reduce PE and TE ADA reactivities when tested on patient serum (Figure 6(B)). Subsequently, both pairs of mutations were applied to Fv3 in scMATCH3 and again seen to efficiently reduce PE and TE ADA reactivities when tested on patient serum (Figure 6(C)). Finally, both pairs of mutations were applied to all Fvs (1 – 3) in scMATCH3 and, also in this case, were seen to efficiently reduce PE and TE ADA reactivities when tested on patient serum (Figure 6(C), right plot, row 3 Supplementary Figure 1). Essentially, the same phenomena could be observed for four additional patients (rows 1, 2, 4, and 5 in Supplementary Figure 1) participating in the study. Importantly, the T_m value for scFv3 with the 67 G-68 G mutation scheme is only slightly reduced (–1.5°C), compared to parental scFv3, while its K_D-value is similar to the parental scFv3 (less than a two-fold difference, Figure 4(B)). Specifically, the 67 G-68 G double-mutation scheme outperformed other mutation pairs that eliminate the CDR2L T-cell epitope, with respect to affinity by more than a factor of 100.

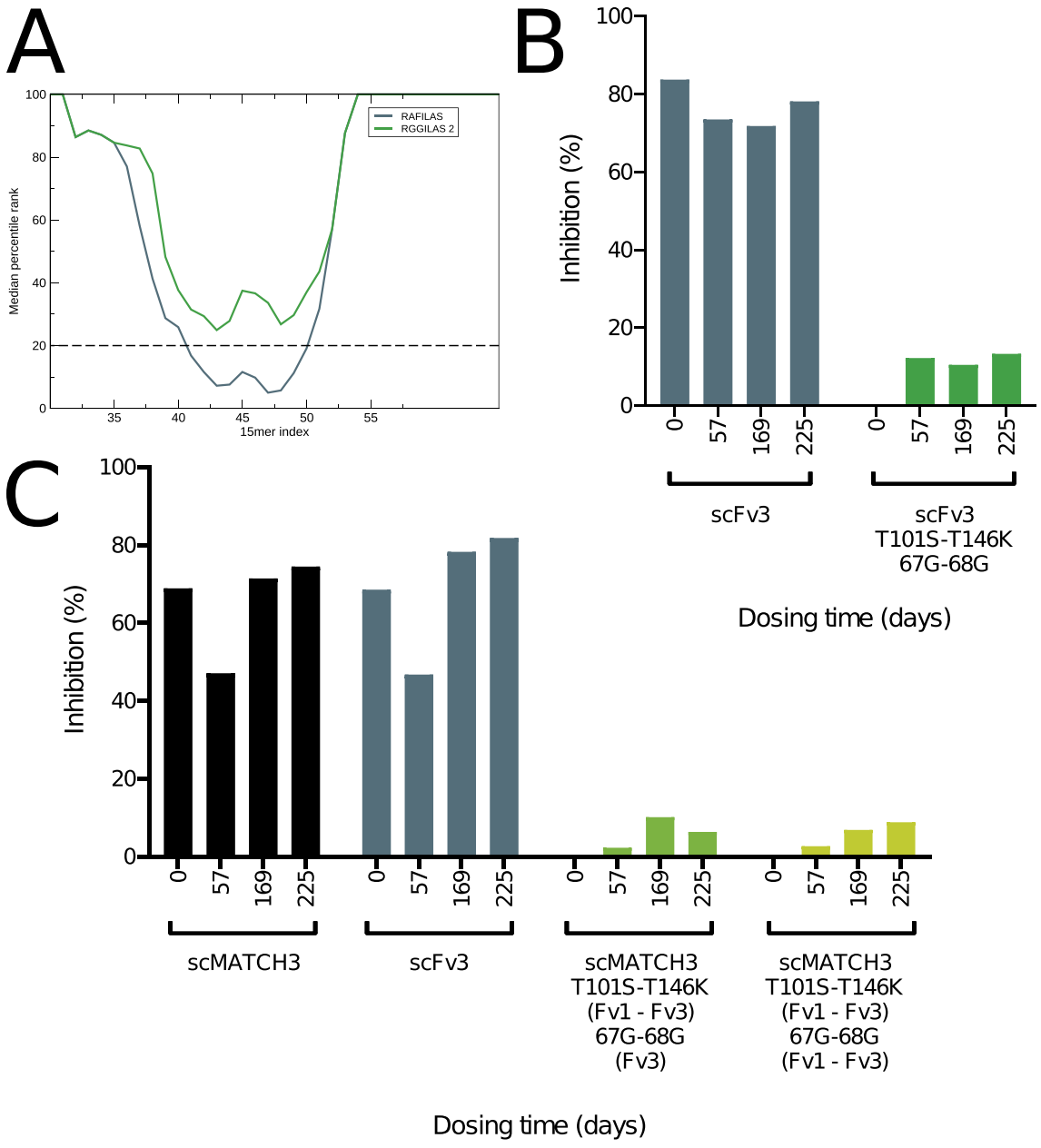

Figure 6. (A) T-cell epitope prediction profiles for scFv3, and scFv3 after application of 67 G-68 G. The median percentile rank of 20 is indicated by a dashed line. (B) Inhibition of absorption signals from day 1 to day 225 after spiking the serum from one patient with scFv3 (450 nM), or scFv3 after application of T101S-T146K and 67 G-68 G (450 nM). (C) Inhibition of absorption signals from day 1 to day 225 after spiking the serum from one patient with scMATCH3 (150 nM), scFv3 only (450 nM), scMATCH3 with T101S-T146K and 67 G-68 G applied to Fv3 (150 nM), and scMATCH3 with T101S-T146K and 67 G-68 G applied to all Fvs (150 nM).

After we showed that the application of the 67 G-68 G mutation scheme to the RAFILAS CDR2L sequence in scFv3 was very successful in terms of reducing TE ADAs (Figure 6(B)), and with only minor impact on thermal stability and affinity (Figure 4(B)), we decided to apply 67 G-68 G to a diverse set of in-house scFvs. We evaluated differences in titer ($n = 64$), monomeric content ($n = 64$), T_m ($n = 75$), and K_D ($n = 88$). For a smaller subset of these scFvs, we evaluated hydrophobicity by hydrophobic interaction chromatography high-performance liquid chromatography (HIC-HPLC, $n = 13$), chemical stability by guanidinium unfolding ($n = 15$), and solubility by polyethylene glycol (PEG) induced precipitation ($n = 10$). For titer and monomeric content (Figures 7(A,B), respectively), no statistically significant difference ($p \geq 0.05$) is observed between scFvs with and without 67 G-68 G (paired Wilcoxon signed rank test). For T_m

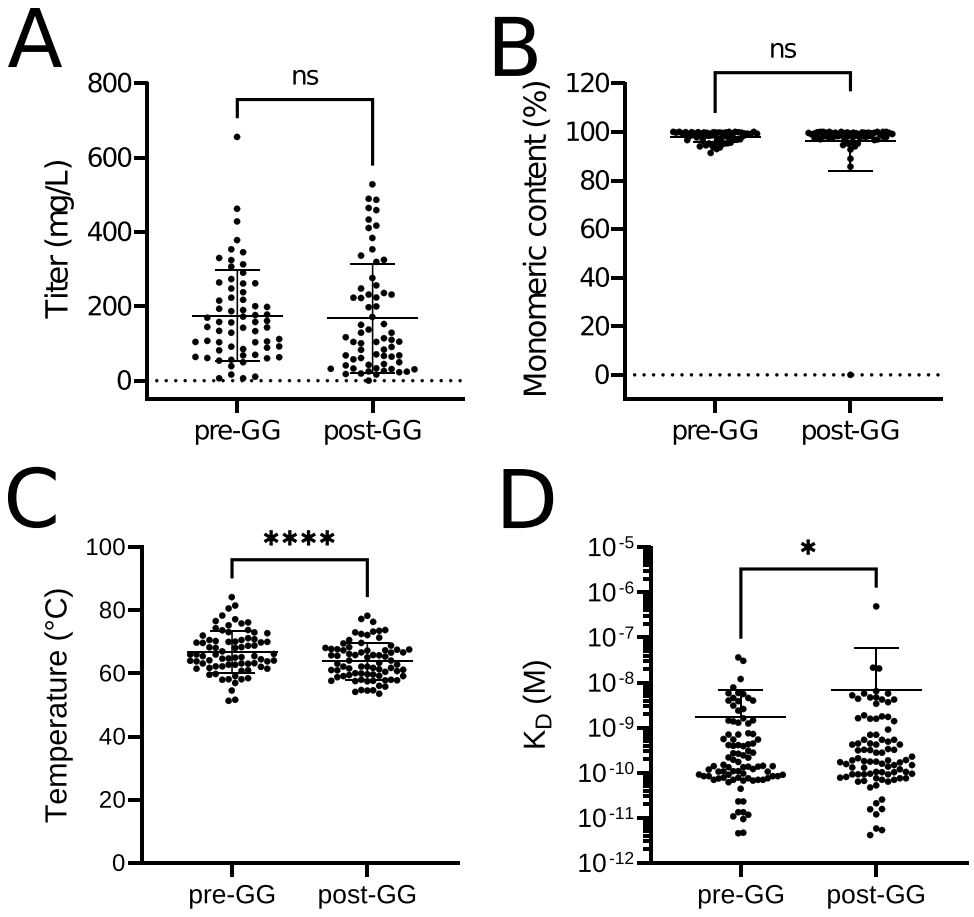

Figure 7. In all panels of this figure, 67 G-68 G is denoted as GG. (A) The final titer (B) and final purity, shows no statistically significant difference is observed between scFvs with and without 67 G-68 G (paired Wilcoxon signed rank test). (C) Melting temperatures of scFvs with and without application of 67 G-68 G. There is a statistically significant Tm difference between scFvs with and without 67 G-68 G ($p < 0.0001$, paired Wilcoxon signed rank test). The scFvs with 67 G-68 G have a lower median melting temperature (−3.1 °c) than their counterparts without 67 G-68 G. (D) Affinities of scFvs with and without application of 67 G-68 G. There is a significant KD difference between scFvs with and without 67 G-68 G ($p = 0.0431$, paired Wilcoxon signed rank test). The scFvs with 67 G-68 G have an overall lower affinity (median 2.3×10^{-11} m) than those without 67 G-68 G.

(Figure 7(C)), there is a statistically significant difference ($p < 0.05$) between scFvs with and without 67 G-68 G (paired Wilcoxon signed rank test). The scFvs with 67 G-68 G have an overall lower T_m (median −3.1°C) than their counterparts without 67 G-68 G. For K_D (Figure 7(D)), there is a statistically significant difference ($p < 0.05$) between scFvs with and without 67 G-68 G (paired Wilcoxon signed rank test). The scFvs with 67 G-68 G have an overall higher K_D (median 2.3×10^{-11} M) compared to those without 67 G-68 G. For hydrophobicity and solubility, there is no statistically significant difference ($p \geq 0.05$) observed for scFvs with and without 67 G-68 G (paired Wilcoxon signed rank test). For chemical stability, there is a statistically significant ($p < 0.05$) difference of −0.29 M guanidinium-HCl observed between scFvs with and without 67 G-68 G (paired Wilcoxon signed rank test).

Evaluation of the 67 G-68 G CDR2L mutation scheme on CSTs

The wider applicability of the 67 G-68 G mutation scheme was tested *in silico* using NetMHCIIpan[44,45] on a set of 962 VL sequences of CSTs. NetMHCIIpan performs predictions using binding affinity (BA) and eluted ligand (EL) models that help with the identification of strong binders and peptides likely to be presented, respectively. The CST sequences were downloaded from the Thera-SabDab database[46] on February 9, 2023. Sequence results are presented as follows: predicted epitopes in version 3.1 [predicted

epitopes in version 4.1 for BA, predicted epitopes in version 4.1 for EL]. Of the 962 CST antibody sequences, 469 [503,490] have a cluster of 15mers with low (< 20) median percentile ranks in CDR2L and application of 67 G-68 G removes the CDR2L cluster for 397 (84.6%) [371 (73.8%), 407 (83.1%)] of these. For the remaining 72 [132, 83] sequences with CDR2L clusters of 15mers with low median percentile ranks, application of 67 G-68 G leads to an increased average CDR2L hotspot – defined as a cluster with a low depth in Materials and methods – minimum value from 5.4 to 13.8 [6.0 to 12.5, 5.1 to 9.2], representing considerably lower predicted risk of immunogenicity. Across all NetMHCIIpan versions used, CDR2L sequences not improved by application of 67 G-68 G are limited to the following five types: LGSNRAS (12.8 to 11.5), DGDFKVY (15 to 13), SASYRYT (8.2 to 7 & 7.7 to 6.9 - note, two results are reported due to different flanking framework residues), HASYRYT (8.0 to 6.9), and SASYVYW (9.7 to 8.0). For clarity of the described results, please refer to Supplementary Figure 2.

Among the 962 VL sequences, there were in total 401 unique CDR2L sequences, of which some are very frequent. For example, AASSLQS (human Vk1_39 germline) is the most frequent CDR2L and found in 59 sequences. Some other common CDR2L sequences are WASTRES (35 occurrences, human Vk4_1 germline), GASSRAT (32 occurrences, human Vk3 germline), DASNRAT (31 occurrences, human Vk3 germline) and KVSNRFS (26 occurrences, human Vk2D_24 germline). Out of the 401 unique CDR2L sequences, the five most common ones occur in 19% of the VL sequences and are human germline sequences considered to be free of immunogenicity risk. Since application of the 67 G-68 G mutation scheme does not substantially impact functional or biophysical properties, it may be a convenient way to mitigate future TE ADA problems, especially when no germline with a suitable residue type on AHo58 exists.

Discussion

In the present study, we investigated the de-immunization of a predicted T-cell MHC class II epitope in CDR2L that provoked the generation of TE ADAs. We showed it is possible to find sets of mutations that eliminate the predicted T-cell epitope content from a specific, problematic CDR2L, without substantially affecting functional or biophysical properties. However, for each new CDR2L sequence with predicted T-cell epitope content, the procedure will typically need to be repeated.

The quantitative occurrence of predicted T-cell epitopes in the CDR2L region of CSTs shows that not all predicted epitopes lead to the generation of critical TE ADAs. Nevertheless, it creates a demand for broadly applicable deimmunization techniques capable of removing predicted T-cell epitopes from the CDR2L region without detrimental effects on either functional or biophysical properties. Indeed, the frequency with which human germline sequences are present in CDR2L of CSTs suggests that these may well have been used as a deimmunization technique for some of these CSTs. In our case however, this leads to AHo58 and three more out of the seven residues in CDR2L being different from the parental CDR2L, and also loss of function and thermal stability. Similar effects from human germline sequences in CDR2L are possible for many other parental sequences and, therefore, a solution in the form of a small and regular mutation scheme for CDR2L that consistently eliminates predicted T-cell epitopes, while not losing functional or biophysical properties, emerges as an attractive proposition compared to the derivation of sequence-specific mutations to eliminate predicted T-cell epitopes. Since all CDR2Ls are equally long in commonly used CDR definitions, and have a similar conformation,[47] the identification of a constant mutation scheme for CDR2L is facilitated. The fact that CDR2L is less crucial for function than, for example CDR3H, is also beneficial.

The 67 G-68 G mutation scheme in CDR2L was, somewhat, surprisingly found to satisfy the requirements of such a solution. We believe that the main reason for this is that 67 G-68 G introduces certain structural flexibility, while the short length and limited conformational variability of CDR2L[47] largely prevents a negative impact on functional or biophysical properties.

The promise of 67 G-68 G is that, regardless of the CDR2L sequence, it largely preserves functional and biophysical properties while eliminating most of the predicted T-cell epitope content. The effectiveness of the mutations was demonstrated by eliminating the binding of generated TE ADAs to the 67 G-68 G CDR2L. This suggests that the 67 G-68 G mutation scheme may be usable as a standard deimmunization device that can be employed, irrespective of whether predicted CDR2L T-cell epitopes are true or false positives. It is important to take into consideration, however, that the majority of the experiments in this study have been conducted using the 67 G-68 G in combination with the mutation scheme to tackle PE

ADAs (T101S-T146K). This was because, during the course of the study, the mutation imposed to eliminate the effect of PE ADAs was integrated into the antibody engineering pipeline. We are aware that this limits the ability to conclude whether the positive effects of 67 G-68 G occur independently or only in combination with T101S-T146K. However, measurements for different CDR2L sequences indicate that modifications in CDR2L alone can fully inhibit TE ADA reactivities, suggesting that T101S-T146K is not a significant contributor to the effects on TE ADA reactivities observed for 67 G-68 G in combination with T101S-T146K.

We believe that since there is currently no method available that excludes false positives at the sequence level, a broadly applicable solution with only minimal effects on functional or biophysical properties would be very useful for avoiding time-consuming identification of clone-specific mutations and/or exclusion of promising sequences/clones.

While we are aware that in silico T-cell epitope prediction methods tend to overpredict false positives, we cannot rule out the possibility of false negatives. Nonetheless, as the examples of this study and Natalizumab[40] have illustrated, while most of the T-cell epitope content of the CDR2L region was predicted as false positives, they should not be discarded lightly as such.

Thus, even if certain immunogenicity predictions prove to be false positives, implementing these mutations effectively mitigates TE ADA risk. The resulting marginal decreases in affinity and thermal stability are a reasonable and worthwhile compromise to ensure patient safety. Therefore, application of mutations, regardless of whether the prediction for immunogenicity may be a false positive, ensures that there is a reduced likeliness of TE ADAs; thereby contributing to the safety profile for patients at a marginally small trade-off with regards to affinity and thermal stability. While this study has concentrated on epitope validation with patient serum ADAs, further studies investigating the stimulation of total patient-derived CD4 memory T cell with autologous APCs and scMATCH3 and the double/quadruple mutants would certainly further validate the approach.

We believe that the method described herein provides a potential means to obtain full-length antibodies as well as antibody fragments with good biophysical properties and reduced immunogenicity for assembly into bispecifics and multispecifics, the latter of which is a topic of increasing interest in recent times.

Materials and methods

Ethics

All patients enrolled in the NM21-1480 clinical trial provided written informed consent prior to participation, in accordance with the principles of the Declaration of Helsinki and Good Clinical Practice (GCP) guidelines. The study protocol and all associated documents were reviewed and approved by the appropriate institutional review boards and ethics committees. This clinical trial was registered at ClinicalTrials.gov (Identifier: NCT04442126).

Proteins

The main protein in this study is a tri-specific scDb-scFv (scMATCH3^{TM}). When an Fv is produced in isolation (including a linker) it is an scFv. Throughout the study, all numbering of residues and sequence positions is according to the AHo numbering scheme.[48] The CDRs of all Fvs/scFvs have rabbit origin, motivated by their high affinity and exceptional sequence diversity,[49–51] and were reformatted into a human Vk1-VH3 consensus type framework stabilized by a so-called lambda (λ)-cap™ of the framework region 4 of the light chain.[49]

Protein expression and purification

Expression plasmids of the scFvs were purchased at GeneUniversal using the pcDNA 3.1 backbone (ThermoFisher Scientific). The expression was performed in Chinese hamster ovary (CHO) cells using the ExpiCHO^{TM} Expression System (ThermoFisher Scientific). Expression was carried out according to manufacturer's instructions. Proteins were purified from clarified harvest by affinity chromatography

(Protein A and/or Protein L) using PrismA and/or Capto^{TM}L resin (Cytiva). When necessary, scFvs were polished by size exclusion (SE) chromatography using a Superdex 75 (Cytiva) to a final monomeric content > 95%.

Expression of scMATCH3^{TM} molecules was performed at 0.5 l scale using CHOgro expression kits (Mirus) and mammalian CHO-S cells. After 7 days of expression, proteins were purified from clarified culture supernatants by Protein A affinity chromatography using MabSelect^{TM} PrismA resin (Cytiva), followed by either SE chromatography in 50 mM phosphate-citrate buffer with 300 mM sucrose at pH 6.5 or, when applicable, capture fractions with > 95% purity were directly pooled and buffer exchanged to 50 mM phosphate-citrate buffer with 300 mM sucrose at pH 6.5 buffer.

Monomeric content determination by size-exclusion HPLC

Monomeric content for the scFvs after purification was assessed using analytical size-exclusion HPLC (SE-HPLC). Samples were applied at their present concentration. 5 µg of scFv were injected into a Shodex KW402.5-4F column using a Hitachi Chromaster HPLC system at 25°C and a flow rate of 0.35 ml/min. The mobile phase consisted of 50 mM sodium acetate, 250 mM sodium chloride, pH 6.0. The elution profile was monitored at 280 nm. Monomeric content for the scMATCH3 molecules was likewise assessed using SE-HPLC.

ADA binding assay

ADAs were detected through analysis of their interactions with coated test molecules (*i.e.*, a scFv or a scMATCH3). The specificity of interactions was assessed by competition of coated test molecules with soluble test molecules. For coating, test molecules were diluted in phosphate-buffered saline (PBS), pH 7.4 (Lonza, #BE17- 517Q) to a concentration of 100 ng/ml, and 25 µl per well were applied onto a 96-well half-area plate (Greiner Bio-One). After incubation for 2 h at room temperature, the wells were blocked for 1 h at room temperature with 150 µl of blocking buffer (PBS +0.2% Tween 20 [AppliChem, #A4974] + 1% BSA [Sigma-Aldrich, #A3294]). For the direct interaction, individual human sera were diluted 20-fold using low cross buffer (Candor, #100 500) and 25 µl applied onto the coated wells at room temperature for 15 min. For the competition with soluble scFvs, individual human sera were diluted 5-fold with low cross buffer, mixed 1:4 with the corresponding test molecule (diluted to 200 nM in low cross buffer) and incubated for 1 h at room temperature prior to applying to the immobilized test molecule as stated above. The minimal required dilution of the assay was at 1:20. For detection, an anti-human Fc-IgG-HRP (Jackson ImmunoResearch, 309–035-008) diluted in low cross buffer to 100 ng/ml was applied and incubated for 1 h at room temperature. 3,3,' 5,5"-tetramethylbenzidine (SeraCare, #5120–0083) was added and the reaction stopped with 1 M HCl (Merck, #1003132500) after 15 minutes at room temperature. Absorbance was measured at 450 nm and 690 nm for reference, using a Tecan plate reader. All steps were performed at room temperature. Between each step, plates were washed three times (PBS, 0.005% Tween 20, pH 7.4). Except for the blocking and washing steps, all assay components were added in a volume of 25 µl/well and duplicates were used. Plates are incubated on a "belly dancer shaker" at 40 rpm.

Thermal stability by nDSF

Thermal unfolding of the molecules was assessed by nDSF using a Prometheus device (Nanotemper Technologies). All proteins were present at 1 ± 0.1 mg/ml in 20 mM histidine buffer, pH 6 (Carl Roth, #3852). Melting curves were generated through a temperature increase from 20°C to 95°C with 1°C/min. Data was analyzed by the PR.ThermControl v2.3.1 and PR.Stability v1.1 software. The first midpoint of unfolding was assessed using the first derivative of the fluorescence ratio (350 nm/330 nm). When possible, all midpoints were assessed.

Hydrophobicity by HIC-HPLC

ScFvs were tested for their hydrophobicity using HIC-HPLC applying a Pro-Pac HIC-10 column (5 µm, 300 Å, 4.6x100 mm, Thermo Fisher 063655). 20 µg of protein are injected and eluted from the column using a gradient from 1.5 M to 0 M $(NH_4)_2SO_4$ (PanReac AppliChem, A1032) in 20 mM Histidine, pH 5.5 (Carl Roth: #9455, PanReac AppliChem: A1341) in 12 minutes with a flow of 1 ml/min. The retention time is subsequently correlated to the respective $(NH_4)_2SO_4$ concentration. For the determination of the $(NH_4)_2SO_4$ concentration, a delay volume of 2.81 ml was applied to account for column volume and dead volume of the system.

Solubility assessment by PEG precipitation assay

ScFvs were tested for their relative solubility using PEG-induced precipitation. ScFvs were incubated at 0.5 mg/ml in 20 mM histidine, pH 6.0 (Carl Roth: #9455, PanReac AppliChem: A1341) with increasing PEG8000 (Sigma-Aldrich: P2139) concentrations from 0% (w/v) to 26.7% (w/v) in 21 steps. After overnight incubation at refrigerated conditions, the optical density at 600 nanometer (OD600nm) was determined. The OD600nm is plotted against the PEG8000 concentration and the midpoint ($PEG_{midpoint}$) of the sigmoidal curve fitted using an in-house script.

Chemical unfolding by guanidinium-HCl

For chemical unfolding experiments, scFvs were incubated in 24 solutions ranging from 0 M to 6.0 M guanidinium-HCl (PanReac AppliChem: A1499) in 20 mM histidine pH 6.0 (Carl Roth: #9455, PanReac AppliChem: A1341). Final protein concentration was 0.10–0.25 mg/ml. Samples were allowed to reach equilibrium overnight at room temperature and were measured for their intrinsic fluorescence at 330 nm and 350 nm using a plate reader (Tecan, Infinite M Plex). The fluorescence ratio (350 nm/330 nm) was plotted against the Guanidinium-HCl concentration and the midpoint of unfolding of the sigmoidal curve fitted using an in-house script.

Binding affinity by SPR

For the determination of the binding kinetics and affinity of the molecules, the respective target proteins for each tested scFv were immobilized on a new CM5 SPR sensor prism chip (Biacore, Cytiva) in a T200 SPR system (Biacore, Cytiva), at the surface density of 100–500 response units with standard amine coupling. The scFv samples were then injected at adapted concentration ranges from 20–30 nM to 150 pM over the ligand-immobilized and reference spots. The parental molecules were measured alongside as controls, while an empty spot was used as reference. After each cycle with analyte, the surface was regenerated with a 3 M $MgCl_2$ solution, thereby allowing the next analyte cycle to have only free ligand available. Dissociation constants (K_D) were globally calculated by the Biacore Evaluation software based on the binding association (k_{on}) and dissociation (k_{off}) rate, by fitting a 1:1 Langmuir model to the curves obtained by the cycles at different analyte concentrations.

T-cell epitope content predictions

MHC class II binding prediction was performed using versions 3.1 and 4.1 of the NetMHCIIpan method,[44,45] obtained from the Immune Epitope Database (IEDB). The NetMHCIIpan version 3.1 method predicts MHC class II binding affinities and their reliabilities for 9-mer cores in contiguous 15mer sub-sequences and individual alleles by application of ensembles feed-forward artificial neural networks[44,52] with 906-neuron input layers, that have been trained on quantitative peptide binding data that covers multiple MHC class II molecules. For the presentation to the 906-neuron input layer of each network, the amino acids of each 9mer core peptide are encoded as the corresponding 20-element vector from the BLOSUM50 matrix.[53] The peptide flanking regions are encoded as one 20-element vector for each side of the binding core, formed as the average BLOSUM50 score vector for the residues in each flanking region.

MHC class II molecules are represented by 34-residue pseudo-sequences, where each residue is again encoded as the corresponding 20-element vector from the BLOSUM50 matrix. Finally, peptide and peptide flanking region lengths are each encoded to two different input neurons. In total this leads to $9 \times 20 + 2 \times 20 + 34 \times 20 + 3 \times 2 = 906$ inputs, for each pair of peptide and MHC class II molecule.

For the prediction results reported herein, a set of 27 alleles was used, which covers a substantial majority of MHC class II molecules.[41] The per-allele percentile rank of a 15mer is obtained from its score by comparing the score against the scores of 200,000 random natural 15mers.[54] For these prediction results, external to the NetMHCIIpan software, any reported 15mer percentile rank for which the 9-mer sequence that gives rise to the 15mer's percentile rank corresponds to a human germline segment, is reset to 100.0 (*i.e.*, a form of germline correction is performed). Thereafter, the median percentile rank for each 15mer sub-sequence is calculated from the 27 per-allele percentile ranks. Longer amino acid sequences are treated by splitting each such sequence into consecutive overlapping contiguous 15mer sub-sequences. Thereafter, the median percentile rank for each 15mer sub-sequence is calculated from the 27 per-allele percentile ranks. A median percentile rank of 20 is commonly seen as broad immunogenicity threshold for the general population,[55] and we use a median percentile rank less than 20 as an indicator of immunogenicity risk, since this is a commonly chosen threshold for this purpose, and compliant with IEDB guidelines for identification of promiscuous peptides.[55,56]

We sometimes refer to the median percentile rank as a function of peptide 15mer index, as a T-cell epitope prediction profile. In such profiles, three or more consecutive values below 20.0 are referred to as a cluster of 15mers with low median percentile ranks. For such a cluster, the total number of consecutive values below 20.0 is known as the cluster width, and if $r_{\min}$ is the lowest value in a cluster, the cluster's depth d, is defined as $d = r_{\min}$. A cluster with a low depth is often referred to as a hotspot. Due to performance improvements for accuracy and allele coverage as a result of more training data, we employed NetMHCIIpan version 4.1 binding affinity (BA) and eluted ligand (EL) models for CSTs, to obtain results from the most current version of NetMCHIIpan at the time of submission and to ensure no significant changes to predictions were present.

Computational procedures

Crystal structures were prepared for Rosetta ΔΔG calculations by removing non-protein compounds including waters and ions, and renumbering residues to start at one and proceed using consecutive integer values. After this, input structures were subjected to energy minimization using harmonic distance constraints on Cα atoms within 9 Å of one another. The ΔΔG prediction calculations themselves were performed by the ddg_monomer application provided in Rosetta (version 2020.08.61164) using the high-resolution protocol,[43] and calculating 50 structures for each mutation. For each mutation or combination of simultaneous mutations, the ddg_monomer application estimates ΔΔG as the difference between the mean of the three top scoring parental structures and the mean of the three top scoring mutant structures.

Graphical representations of molecular structures were generated with UCSF Chimera[57,58] and heatmaps were generated with R[59] using the ComplexHeatmap package.[60] A contact between two atoms, i and j, is identified by Chimera as being present when the so-called overlap ($overlap_{ij}$) between the two atoms i and j is greater than or equal to −0.4 Å, where $overlap_{ij}$ is defined by $overlap_{ij} = r_i^{\mathrm{VdW}} + r_j^{\mathrm{VdW}} - d_{ij}$, where r_i^{VdW} and r_j^{VdW} denotes the Van der Waals radius[61] of atom i and atom j, respectively, and d_{ij} denotes the distance between atom i and atom j.

Abbreviations

ADA:	anti-drug antibody
AHo:	Honegger
CDR:	complementary-determining region
CDR2L:	second complementary-determining region of the light chain

CHO:	Chinese hamster ovary
CST:	clinical-stage therapeutics
nDSF:	nano differential scanning fluorimetry
FDA:	Food and Drug Administration
HIC-HPLC:	hydrophobic interaction chromatography-high-performance liquid chromatography
Fv:	variable fragment
HIC:	hydrophobic interaction chromatography
HPLC	high-performance liquid chromatography
IEDB	Immune Epitope Database
MHC:	major histocompatibility complex
MoA:	mechanism of action
PBS:	phosphate-buffered saline
PE:	preexisting
PEG:	polyethylene glycol
pI:	isoelectric point
PTM:	post-translational modifications
RCSB PDB:	Research Collaboratory for Structural Bioinformatics Protein Data Bank
scDb-scFv:	single-chain diabody fused to a single-chain Fv
scFv:	single-chain variable fragment
scMATCH3:	single-chain diabody fused to a single-chain Fv
SE:	size exclusion
SE-HPLC:	size-exclusion-high-performance liquid chromatography
SPR:	surface plasmon resonance
TE:	treatment-emergent
VH:	variable heavy chain
VL:	variable light chain

Acknowledgments

The authors want to thank Numab Therapeutics coworkers that have been involved in lab support and scientific discussions related to this work. We also thank Josephine Adams for her contribution to the preparation of the ethics statement.

Disclosure statement

This research was funded by Numab Therapeutics AG. The authors were all employed by Numab Therapeutics AG at the time when the study was conducted.

Funding

The author(s) reported there is no funding associated with the work featured in this article.

ORCID

Fabio Mario Spiga http://orcid.org/0000-0002-0541-3141
Julia Tietz http://orcid.org/0009-0006-5103-0842
Christopher Weinert http://orcid.org/0000-0003-3313-9458
Christian Hess http://orcid.org/0009-0006-4556-6288
David Urech http://orcid.org/0009-0003-2167-7440
Stefan Warmuth http://orcid.org/0000-0001-6872-8805

Author contributions

Conceptualization – MUJ, SW; Investigation – MUJ, AK, AC, SC, YS, ADF, DM, MT, FMS, JT, CW, CH, SW; Original draft preparation – MUJ; Figures and visualizations – MUJ, AK, SC, SW; Review and editing – MUJ, SC, ADF, FMS, CW, CH, DU, SW.

References

1. Immunogenicity information in human prescription therapeutic protein and select drug product labeling — content and format, guidance for industry. Department of Health and Human Services, Food and Drug Administration. https://www.Fda.gov/media/155871/download.
2. Harris CT, Cohen S. Reducing immunogenicity by design: approaches to minimize immunogenicity of monoclonal antibodies. BioDrugs. 2024;38(2):205–226. doi: 10.1007/s40259-023-00641-2 PMID: 38261155.
3. Shankar G, Arkin S, Cocea L, Devanarayan V, Kirshner S, Kromminga A, Quarmby V, Richards S, Schneider CK, Subramanyam M, et al. Assessment and reporting of the clinical immunogenicity of therapeutic proteins and peptides-harmonized terminology and tactical recommendations. Aaps J. 2014;16(4):658–673. doi: 10.1208/s12248-014-9599-2 PMID: 24764037.
4. Mullins GR, Ardayfio P, Gueorguieva I, Anglin G, Bailey J, Chua L, Zimmer JA, Evans CD, Nery ESM, Wang H, et al. Donanemab immunogenicity in participants with early symptomatic Alzheimer's disease. Alzheimers Dement (NY). 2025;11(3):e70149. doi: 10.1002/trc2.70149 PMID: 40904419.
5. Mullins GR, Hodsdon ME, Li YG, Anglin G, Urva S, Schneck K, Bardos JN, Martins RF, Brown K, Calderon B. Tirzepatide immunogenicity on pharmacokinetics, efficacy, and safety: analysis of data from phase 3 studies. J Clin Endocrinol Metab. 2024;109(2):361–369. doi: 10.1210/clinem/dgad532 PMID: 37700637.
6. Martinez JM, Hindiyeh N, Anglin G, Kalidas K, Hodsdon ME, Kielbasa W, Moser BA, Pearlman EM, Garces S. Assessment of immunogenicity from galcanezumab phase 3 trials in patients with episodic or chronic migraine. Cephalalgia. 2020;40(9):978–989. doi: 10.1177/0333102420920642 PMID: 32340471.
7. Koren E, Zuckerman LA, Mire-Sluis AR. Immune responses to therapeutic proteins in humans–clinical significance, assessment and prediction. Curr Pharm Biotechnol. 2002;3(4):349–360. doi: 10.2174/1389201023378175 PMID: 12463417.
8. Kuus-Reichel K, Grauer LS, Karavodin LM, Knott C, Krusemeier M, Kay NE. Will immunogenicity limit the use, efficacy, and future development of therapeutic monoclonal antibodies? Clin Diagn Lab Immunol. 1994;1(4):365–372. doi: 10.1128/cdli.1.4.365-372.1994 PMID: 8556470.
9. Schellekens H, Casadevall N. Immunogenicity of recombinant human proteins: causes and consequences. J Neurol. 2004;Suppl 251(S2):II4–9. doi: 10.1007/s00415-004-1202-9 PMID: 15264106.
10. Guidance for industry, immunogenicity assessment for therapeutic protein products. U.S. Department of Health and Human Services, Food and Drug Administration; 2014. https://www.fda.gov/media/85017/download.
11. Guideline on Immunogenicity assessment of therapeuticproteins. 2017. https://www.ema.europa.eu/en/documents/scientific-guideline/guideline-immunogenicity-assessment-therapeutic-proteins-revision-1_en.pdf.
12. Callahan MKYA, Xu S, Tandon Y, Subudhi SK, Roman RA, Heine AI, Kuk E, Pogoriler D, Yuan K, Panageas JD, et al. Evaluation of serum IL-17 levels during ipilimumab therapy: correlation with colitis. J Clin Oncol. 2011;29(15_suppl):2505–2505. doi: 10.1200/jco.2011.29.15_suppl.2505
13. Davda J, Declerck P, Hu-Lieskovan S, Hickling TP, Jacobs IA, Chou J, Salek-Ardakani S, Kraynov E. Immunogenicity of immunomodulatory, antibody-based, oncology therapeutics. J Immunother Cancer. 2019;7(1):105. doi: 10.1186/s40425-019-0586-0 PMID: 30992085.
14. Harding FA, Stickler MM, Razo J, DuBridge RB. The immunogenicity of humanized and fully human antibodies: residual immunogenicity resides in the CDR regions. MAbs. 2010;2(3):256–265. doi: 10.4161/mabs.2.3.11641 PMID: 20400861.
15. Boehncke WH, Brembilla NC. Immunogenicity of biologic therapies: causes and consequences. Expert Rev Clin Immunol. 2018;14(6):513–523. doi: 10.1080/1744666X.2018.1468753 PMID: 29683362.
16. Dingman R, Balu-Iyer SV. Immunogenicity of protein pharmaceuticals. J Pharm Sci. 2019;108(5):1637–1654. doi: 10.1016/j.xphs.2018.12.014 PMID: 30599169.
17. Pineda C, Castaneda Hernandez G, Jacobs IA, Alvarez DF, Carini C. Assessing the immunogenicity of biopharmaceuticals. BioDrugs. 2016;30(3):195–206. doi: 10.1007/s40259-016-0174-5 PMID: 27097915.
18. Singh SK. Impact of product-related factors on immunogenicity of biotherapeutics. J Pharm Sci. 2011;100(2):354–387. doi: 10.1002/jps.22276 PMID: 20740683.
19. Gopal AK, Kahl BS, Flowers CR, Martin P, Ansell SM, Abella-Dominicis E, Koh B, Ye W, Barr PM, Salles GA, et al. Idelalisib is effective in patients with high-risk follicular lymphoma and early relapse after initial chemoimmunotherapy. Blood. 2017;129(22):3037–3039. doi: 10.1182/blood-2016-12-757740 PMID: 28325864.
20. Ruperto N, Bazso A, Ravelli A, Malattia C, Filocamo G, Pistorio A, Rodriguez Lozano AL, Viola S, Martini A. Paediatric rheumatology International trials O. The paediatric rheumatology International trials organization (PRINTO). Lupus. 2007;16(8):670–676. doi: 10.1177/0961203307079556 PMID: 17711906.
21. Jawa V, Cousens LP, Awwad M, Wakshull E, Kropshofer H, De Groot AS. T-cell dependent immunogenicity of protein therapeutics: preclinical assessment and mitigation. Clin Immunol. 2013;149(3):534–555. doi: 10.1016/j.clim.2013.09.006 PMID: 24263283.
22. Benucci M, Damiani A, Li Gobbi F, Bandinelli F, Infantino M, Grossi V, Manfredi M, Noguier G, Meacci F. Correlation between HLA haplotypes and the development of antidrug antibodies in a cohort of patients with rheumatic diseases. Biologics. 2018;12:37–41. doi: 10.2147/BTT.S145941 PMID: 29430171.

23. Duke BR, Mitra-Kaushik S. Current in vitro assays for prediction of T cell mediated immunogenicity of biotherapeutics and manufacturing impurities. J Pharm Innov. 2020;15(2):202–218. doi: 10.1007/s12247-019-09412-5
24. Moussa EM, Panchal JP, Moorthy BS, Blum JS, Joubert MK, Narhi LO, Topp EM. Immunogenicity of therapeutic protein aggregates. J Pharm Sci. 2016;105(2):417–430. doi: 10.1016/j.xphs.2015.11.002 PMID: 26869409.
25. Rosenberg AS. Effects of protein aggregates: an immunologic perspective. Aaps J. 2006;8(3):E501–507. doi: 10.1208/aapsj080359 PMID: 17025268.
26. Liu L. Pharmacokinetics of monoclonal antibodies and Fc-fusion proteins. Protein Cell. 2018;9(1):15–32. doi: 10.1007/s13238-017-0408-4 PMID: 28421387.
27. Doyle HA, Gee RJ, Mamula MJ. Altered immunogenicity of isoaspartate containing proteins. Autoimmunity. 2007;40(2):131–137. doi: 10.1080/08916930601165180 PMID: 17453712.
28. Eggleton P, Haigh R, Winyard PG. Consequence of neo-antigenicity of the 'altered self'. Rheumatol (Oxford). 2008;47(5):567–571. doi: 10.1093/rheumatology/ken014 PMID: 18316337.
29. Chirino AJ, Ary ML, Marshall SA. Minimizing the immunogenicity of protein therapeutics. Drug Discov Today. 2004;9(2):82–90. doi: 10.1016/S1359-6446(03)02953-2 PMID: 15012932.
30. Schellekens H. How to predict and prevent the immunogenicity of therapeutic proteins. Biotechnol Annu Rev. 2008;14:191–202. doi: 10.1016/S1387-2656(08)00007-0 PMID: 18606364.
31. Hill JA, Wang D, Jevnikar AM, Cairns E, Bell DA. The relationship between predicted peptide-MHC class II affinity and T-cell activation in a HLA-DRbeta1*0401 transgenic mouse model. Arthritis Res Ther. 2003;5(1):R40–48. doi: 10.1186/ar605 PMID: 12716452.
32. Lazarski CA, Chaves FA, Jenks SA, Wu S, Richards KA, Weaver JM, Sant AJ. The kinetic stability of MHC class II: peptide complexes is a key parameter that dictates immunodominance. Immunity. 2005;23(1):29–40. doi: 10.1016/j.immuni.2005.05.009 PMID: 16039577.
33. Wang P, Sidney J, Dow C, Mothe B, Sette A, Peters B. A systematic assessment of MHC class II peptide binding predictions and evaluation of a consensus approach. PLoS Comput Biol. 2008;4(4):e1000048. doi: 10.1371/journal.pcbi.1000048 PMID: 18389056.
34. van der Merwe PA, Davis SJ. Molecular interactions mediating T cell antigen recognition. Annu Rev Immunol. 2003;21(1):659–684. doi: 10.1146/annurev.immunol.21.120601.141036 PMID: 12615890.
35. Wang P, Sidney J, Kim Y, Sette A, Lund O, Nielsen M, Peters B. Peptide binding predictions for HLA DR, DP and DQ molecules. BMC Bioinf. 2010;11(1):568. doi: 10.1186/1471-2105-11-568 PMID: 21092157.
36. Andreatta M, Trolle T, Yan Z, Greenbaum JA, Peters B, Nielsen M. An automated benchmarking platform for MHC class II binding prediction methods. Bioinformatics. 2018;34(9):1522–1528. doi: 10.1093/bioinformatics/btx820 PMID: 29281002.
37. Mazor R, Tai CH, Lee B, Pastan I. Poor correlation between T-cell activation assays and HLA-DR binding prediction algorithms in an immunogenic fragment of Pseudomonas exotoxin A. J Immunol Methods. 2015;425:10–20. doi: 10.1016/j.jim.2015.06.003 PMID: 26056938.
38. Zhang H, Lundegaard C, Nielsen M. Pan-specific MHC class I predictors: a benchmark of HLA class I pan-specific prediction methods. Bioinformatics. 2009;25(1):83–89. doi: 10.1093/bioinformatics/btn579 PMID: 18996943.
39. Johansson MU, Weinert C, Reichardt DA, Mahler D, Diem D, Hess C, Feusi D, Carnal S, Tietz J, Giezendanner N, et al. Design of antibody variable fragments with reduced reactivity to preexisting anti-drug antibodies. MAbs. 2023;15(1):2215887. doi: 10.1080/19420862.2023.2215887 PMID: 37312434.
40. Cassotta A, Mikol V, Bertrand T, Pouzieux S, Le Parc J, Ferrari P, Dumas J, Auer M, Deisenhammer F, Gastaldi M, et al. A single T cell epitope drives the neutralizing anti-drug antibody response to natalizumab in multiple sclerosis patients. Nat Med. 2019;25(9):1402–1407. doi: 10.1038/s41591-019-0568-2 PMID: 31501610.
41. Greenbaum J, Sidney J, Chung J, Brander C, Peters B, Sette A. Functional classification of class II human leukocyte antigen (HLA) molecules reveals seven different supertypes and a surprising degree of repertoire sharing across supertypes. Immunogenetics. 2011;63(6):325–335. doi: 10.1007/s00251-011-0513-0 PMID: 21305276.
42. Weber CA, Mehta PJ, Ardito M, Moise L, Martin B, De Groot AS. T cell epitope: friend or foe? Immunogenicity of biologics in context. Adv Drug Deliv Rev. 2009;61(11):965–976. doi: 10.1016/j.addr.2009.07.001 PMID: 19619593.
43. Kellogg EH, Leaver-Fay A, Baker D. Role of conformational sampling in computing mutation-induced changes in protein structure and stability. Proteins. 2011;79(3):830–838. doi: 10.1002/prot.22921 PMID: 21287615.
44. Andreatta M, Karosiene E, Rasmussen M, Stryhn A, Buus S, Nielsen M. Accurate pan-specific prediction of peptide-MHC class II binding affinity with improved binding core identification. Immunogenetics. 2015;67(11–12):641–650. doi: 10.1007/s00251-015-0873-y PMID: 26416257.
45. Reynisson B, Alvarez B, Paul S, Peters B, Nielsen M. NetMHCpan-4.1 and NetMHCIIpan-4.0: improved predictions of MHC antigen presentation by concurrent motif deconvolution and integration of MS MHC eluted ligand data. Nucleic Acids Res. 2020;48(W1):W449–W454. doi: 10.1093/nar/gkaa379 PMID: 32406916.

46. Raybould MIJ, Marks C, Lewis AP, Shi J, Bujotzek A, Taddese B, Deane CM. Thera-SAbDab: the therapeutic structural antibody database. Nucleic Acids Res. 2020;48(D1):D383–D388. doi: 10.1093/nar/gkz827 PMID: 31555805.
47. Teplyakov A, Obmolova G, Malia TJ, Luo J, Muzammil S, Sweet R, Almagro JC, Gilliland GL. Structural diversity in a human antibody germline library. MAbs. 2016;8(6):1045–1063. doi: 10.1080/19420862.2016.1190060 PMID: 27210805.
48. Honegger A, Pluckthun A. Yet another numbering scheme for immunoglobulin variable domains: an automatic modeling and analysis tool. J Mol Biol. 2001;309(3):657–670. doi: 10.1006/jmbi.2001.4662 PMID: 11397087.
49. Egan TJ, Diem D, Weldon R, Neumann T, Meyer S, Urech DM. Novel multispecific heterodimeric antibody format allowing modular assembly of variable domain fragments. MAbs. 2017;9(1):68–84. doi: 10.1080/19420862.2016.1248012 PMID: 27786600.
50. Lavinder JJ, Hoi KH, Reddy ST, Wine Y, Georgiou G. Systematic characterization and comparative analysis of the rabbit immunoglobulin repertoire. PLOS ONE. 2014;9(6):e101322. doi: 10.1371/journal.pone.0101322 PMID: 24978027.
51. Rader C, Ritter G, Nathan S, Elia M, Gout I, Jungbluth AA, Cohen LS, Welt S, Old LJ, Barbas CF 3rd. The rabbit antibody repertoire as a novel source for the generation of therapeutic human antibodies. J Biol Chem. 2000;275(18):13668–13676. doi: 10.1074/jbc.275.18.13668 PMID: 10788485.
52. Nielsen M, Justesen S, Lund O, Lundegaard C, Buus S. NetMHCIIpan-2.0 - improved pan-specific HLA-DR predictions using a novel concurrent alignment and weight optimization training procedure. Immunome Res. 2010;6(1):9. doi: 10.1186/1745-7580-6-9 PMID: 21073747.
53. Henikoff S, Henikoff JG. Amino acid substitution matrices from protein blocks. Proc Natl Acad Sci USA. 1992;89(22):10915–10919. doi: 10.1073/pnas.89.22.10915 PMID: 1438297.
54. Karosiene E, Rasmussen M, Blicher T, Lund O, Buus S, Nielsen M. NetMHCIIpan-3.0, a common pan-specific MHC class II prediction method including all three human MHC class II isotypes, HLA-DR, HLA-DP and HLA-DQ. Immunogenetics. 2013;65(10):711–724. doi: 10.1007/s00251-013-0720-y PMID: 23900783.
55. Paul S, Lindestam Arlehamn CS, Scriba TJ, Dillon MB, Oseroff C, Hinz D, McKinney DM, Carrasco Pro S, Sidney J, Peters B, et al. Development and validation of a broad scheme for prediction of HLA class II restricted T cell epitopes. J Immunol Methods. 2015;422:28–34. doi: 10.1016/j.jim.2015.03.022 PMID: 25862607.
56. Oseroff C, Sidney J, Kotturi MF, Kolla R, Alam R, Broide DH, Wasserman SI, Weiskopf D, McKinney DM, Chung JL, et al. Molecular determinants of T cell epitope recognition to the common Timothy grass allergen. J Immunol. 2010;185(2):943–955. doi: 10.4049/jimmunol.1000405 PMID: 20554959.
57. Pettersen EF, Goddard TD, Huang CC, Couch GS, Greenblatt DM, Meng EC, Ferrin TE. UCSF Chimera–a visualization system for exploratory research and analysis. J Comput Chem. 2004;25(13):1605–1612. doi: 10.1002/jcc.20084 PMID: 15264254.
58. Pettersen EF, Goddard TD, Huang CC, Meng EC, Couch GS, Croll TI, Morris JH, Ferrin TE. Ucsf chimerax: structure visualization for researchers, educators, and developers. Protein Sci. 2021;30(1):70–82. doi: 10.1002/pro.3943 PMID: 32881101.
59. R Development Core Team. R: a language and environment for statistical computing. [software] Vienna, Austria: R Foundation for Statistical Computing; 2010.
60. Gu Z. Complex heatmap visualization. iMeta. 2022;1(3). doi: 10.1002/imt2.43
61. Tsai J, Taylor R, Chothia C, Gerstein M. The packing density in proteins: standard radii and volumes. J Mol Biol. 1999;290(1):253–266. doi: 10.1006/jmbi.1999.2829 PMID: 10388571.